Fabrication of Size-Controllable and Arrangement-Orderly HepG2 Spheroids for Drug Screening via Decellularized Liver Matrix-Derived Micropattern Array Chips

Xinglong Zhu,[○] Qiong Wu,[○] Yuting He, Mengyu Gao, Yi Li, Wanliu Peng, Shengfu Li, Yong Liu, Rundong Zhang, and Ji Bao*

ACCESS | Metrics & More | Article Recommendations | SI Supporting Information

ABSTRACT: Three-dimensional (3D) culture via micropattern arrays to generate cellular spheroids seems a promising *in vitro* biomimetic system for liver tissue engineering applications, such as drug screening. Recently, organ-derived decellularized extracellular matrix emerges as arguably the most biomimetic bioink. Herein, decellularized liver matrix (DLM)-derived micropattern array chips were developed to fabricate size-controllable and arrangement-orderly HepG2 spheroids for drug screening. The porcine DLM was obtained by the removal of cellular components and then ground into powder, followed by enzymolysis. DLM as a coating substrate was compared with collagen type I (Col I) and Matrigel in terms of biological performance for enhancing cell adhesion, proliferation, and functions. Subsequently, we used poly(dimethylsiloxane) (PDMS) to adsorb DLM as the bioink to fabricate micropattern array chips. The optimal shape and size of micropattern were determined by evaluating the morphology, viability, and functions of HepG2 3D cellular aggregates. In addition, drug-susceptibility testing (paclitaxel, doxorubicin HCl, and disulfiram) was performed on this novel platform. The DLM provided the tissue-specific microenvironment that provided suitable supports for HepG2 cells, compared to Col I and Matrigel. A circular micropattern with a diameter of 100 μm was the optimal processing parameter to rapidly fabricate large-scale, size-controllable, and arrangement-orderly HepG2 cellular aggregates with 3D spheroid's shape and high cell viability. Drug screening testing showed that the effect of a drug could be directly demonstrated on-chip by confocal microscopy measuring the viability of spheroids. We provide a novel platform for the large-scale generation of HepG2 spheroids with uniform size and arrangement, thus bringing convenience, reducing error, and increasing reproducibility for a rapid drug discovery by fluorescence quantitative analysis. This methodology may be possible to apply in advancing personalized medicine and drug discovery.
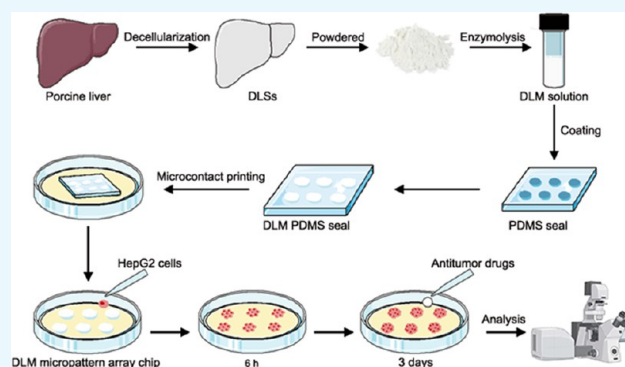
1. INTRODUCTION

Liver cancer is among the most fatal malignant tumors, with an ever-increasing annual percentage globally. Currently, chemotherapy is one of the primary therapeutic options for hepatocellular carcinomas (HCCs) treatment.[1] For decades, the traditional two-dimensional (2D) culture platforms have been widely used in high-throughput antihepatoma compounds and drug screening.[2] Nevertheless, the models lack the intricate microenvironment of native tumors, including cell−cell and cell−extracellular matrix interactions, which are crucial factors to affect cell fate.[3] Moreover, 2D monolayered cells cannot mimic biochemical concentration gradients *in vivo* because they are exposed to a uniform concentration of factors due to direct contact with the culture medium.[4] Conversely, three-dimensional (3D) tumor spheroids could significantly improve the viability, histomorphology, genotype stability, function, and drug metabolism of tumor cells *in vitro*.[5] Their rearrangement and compaction of cell aggregates are

surrounded by a natural extracellular matrix (ECM), which better replicates the microenvironment of solid tumors *in vivo*.[6] Furthermore, tumor spheroids exhibited higher drug resistance of anticancer drugs than 2D models and are promising in the prediction of drug penetration widely overlooked.[3]

The applications of tumor spheroids have been limited by many factors, such as cost and reproducibility. Different spheroids culturing techniques will influence the spheroids' shape, size, surface features, internal textures, and density. Especially, the shape and size of spheroids can affect the
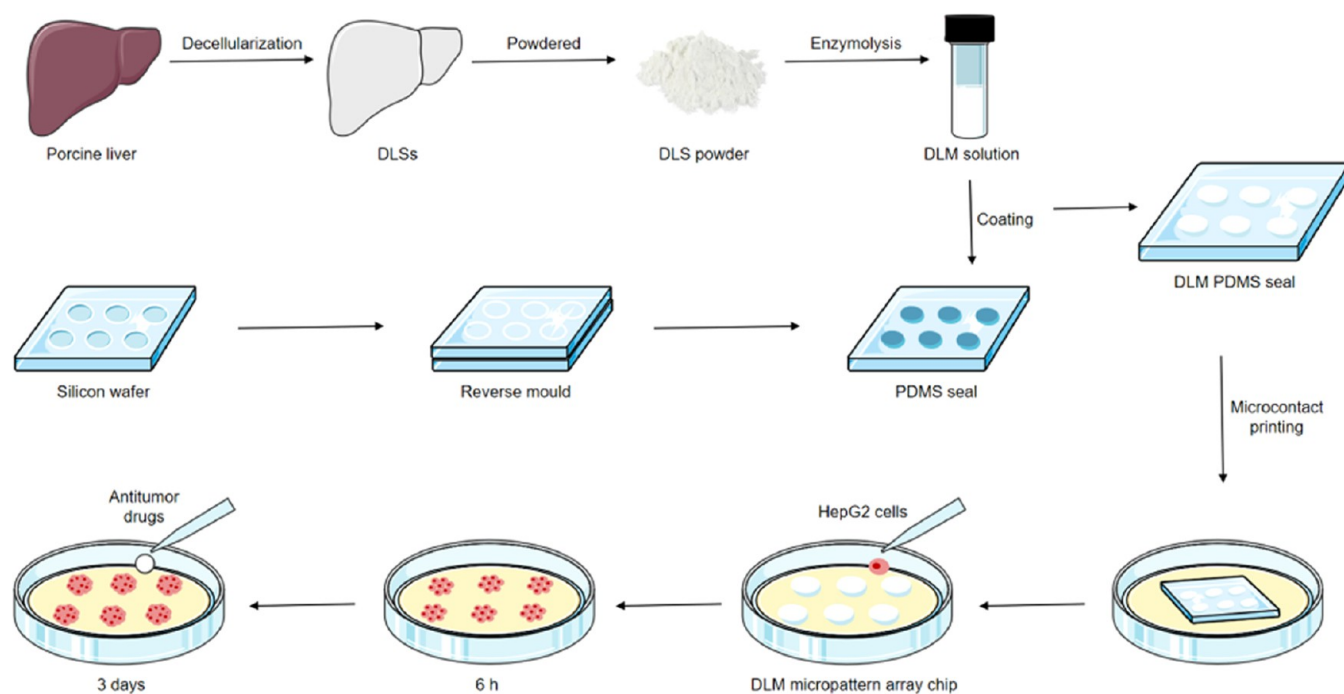
Figure 1. Schematic illustration of DLM micropattern array chips to fabricate HepG2 spheroids for drug screening. DLSs (decellularized liver scaffolds); DLM (decellularized liver matrix); PDMS (poly(dimethylsiloxane)).
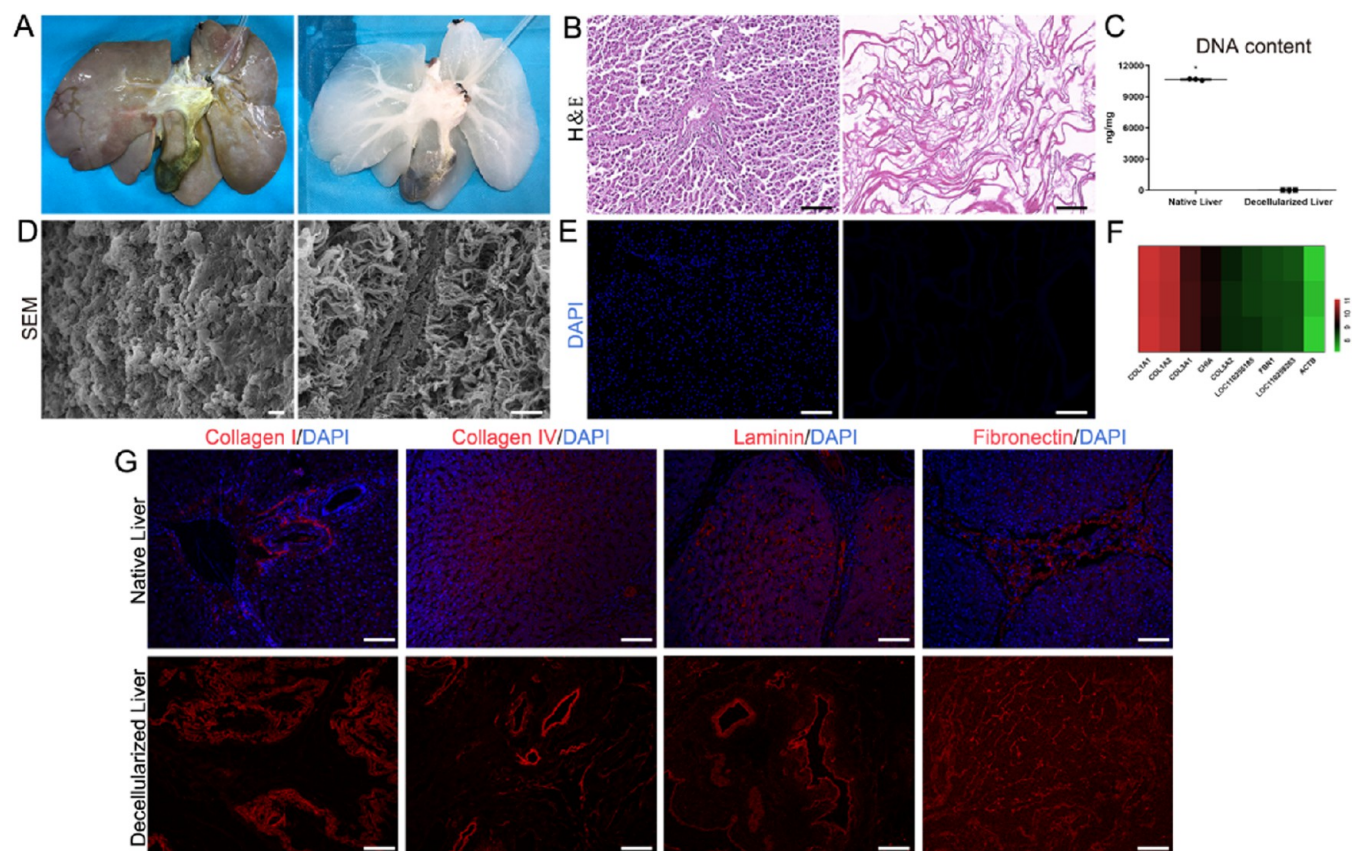

Figure 2. Characteristics of porcine DLM. (A) Macroscopic view of the native and decellularized liver. (B) Hematoxylin and eosin (H&E) staining of native liver and DLM. (C) Quantification of DNA content in native liver and DLM ($n = 3$, *$p < 0.05$). (D) Electron microscopy (SEM) images of native liver and DLM. (E) 4′,6-Diamidino-2-phenylindole (DAPI) staining of native liver and DLM. (F) Protein composition of DLM ($n = 3$). (G) Immunohistochemistry (red) for DLM proteins (collagen I, collagen IV, laminin, and fibronectin) of native liver and DLM; the nuclei were counterstained with DAPI (blue). Scale bars of B, E, and G = 100 μm; scale bar of D = 10 μm.
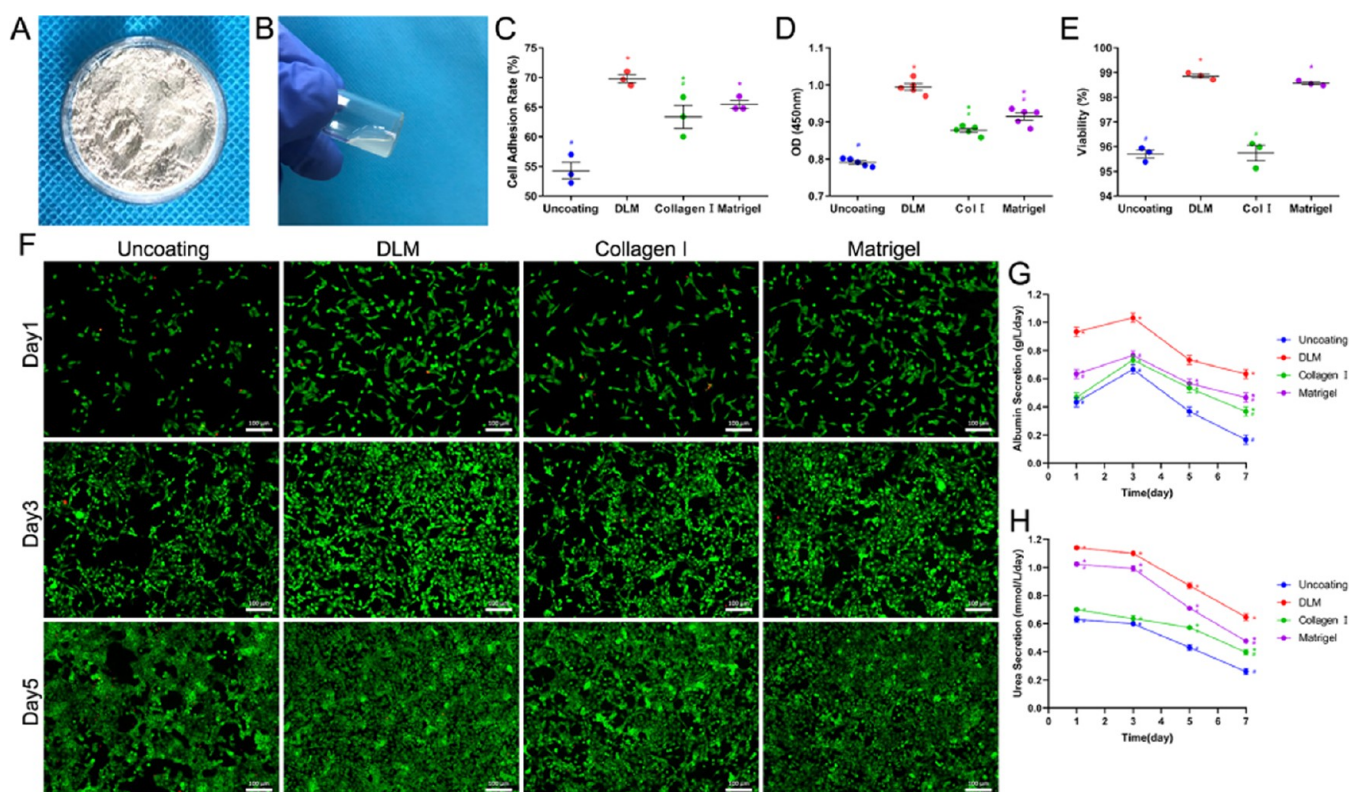
Figure 3. Preparation of soluble DLM and culture of HepG2 cells on DLM-coated substrates. (A) Powder of DLM. (B) Soluble DLM. (C) Number of HepG2 cells adhesion rate onto each substrate at 4 h after cell seeding. (D) Proliferation of HepG2 cells (cck-8) onto the substrates on day 1 after cell seeding. (E) Viability of HepG2 cells cultured on each substrate ($n = 3$). (F) Live/Dead staining of HepG2 cells cultured on each substrate on days 1, 3, and 5. (G) Quantification of albumin secretion from hepatocytes cultured on each substrate using a human albumin ELISA kit ($n = 3$). Quantification of urea synthesis by HepG2 cells cultured on each substrate using the urea assay kit ($n = 3$). Each substrate (noncoated, DLM, Col I, and Matrigel-coated substrate). *$p < 0.05$, compared to the noncoated group, #$p < 0.05$, compared to the DLM-coated group, scale bar = 100 μm.

outcome of drug delivery and efficacy.[7,8] Consequently, it is necessary to modulate the concordance of spheroids' morphological characteristics to reduce error and increase reproducibility. The tumor spheroid culturing methods include the hanging drop method, matrix encapsulation culturing, spinner flasks culturing, ultralow attachment plates, rocked suspension culture techniques, microfluidics, microwell meshes, magnetic levitation, and 3D-printing technology.[9−12] However, these methods are difficult to control the size and arrangement of tumor spheroids, thereby causing difficulties in observing and analyzing tumor spheroids. They also cause low efficiency and poor repeatability of drug screening.[2] Micropatterned arrays formed by covalently or noncovalently coating carbohydrates, peptides, and proteins form patterned arrangements of the definite shape and size on planar substrates.[13] Cells are restrictively adhered to the micropattern, resulting in limited cell growth. Furthermore, cells will spontaneously assemble into spheroids with a 3D multicellular structure by the proliferation of cells and cell−cell adhesion abilities.[14] These arrangements enable culturing a controllable size and orderly arrangement of 3D multicellular spheroids for high-throughput screening. Poly(dimethylsiloxane) (PDMS)-adsorbed proteins (as a bioink) create protein-specific microarrays on nonattachment plates by microcontact printing technology.[15,16] These plates have been widely used in cytology, drug screening, and tissue engineering.[17] Fibronectin, collagen I, collagen IV, and laminin as bioinks are mainly used for the traditional micropattern array.[18,19] However, the single

ECM protein component is not enough to improve and regulate the viability and functions of specific cell lines, primary cells, or induced pluripotent stem cell (iPSC)-derived differentiated cells.[20]

Recent advances in whole organ and tissue decellularization have made it possible to obtain organ-specific ECM with unique architecture, composition, and biological and physical properties.[21−23] Compared with a single ECM protein component, such as collagen I which was widely used in the liver tissue engineering, liver-specific ECM containing various biomacromolecules directs signal molecules or interacts with tumor cells through integrins, discoidin domain receptors (DDRs), and transmembrane protein proteoglycans to regulate the signaling pathways related to cell proliferation, migration, and differentiation, thereby influencing the cells' biological behavior.[24,25]

Herein, we assessed the reservation and categories of biomacromolecules in decellularized liver matrix (DLM) after decellularization. HepG2 cells cultured on the DLM as coating substrate exhibited a higher cell adhesion rate, viability, proliferation, and functions than Matrigel and Col I. HepG2 cellular aggregates were fabricated by combining the patterned microarray and DLM as the bioink. The effects of the shape (round and square) and diameter (50, 75, 100, 150, 200, and 300 μm) of the patterned microarray on the morphology, homogeneity, viability, and functions of HepG2 cellular aggregates were then explored. HepG2 spheroids on DLM micropattern arrays were subsequently used as a testing
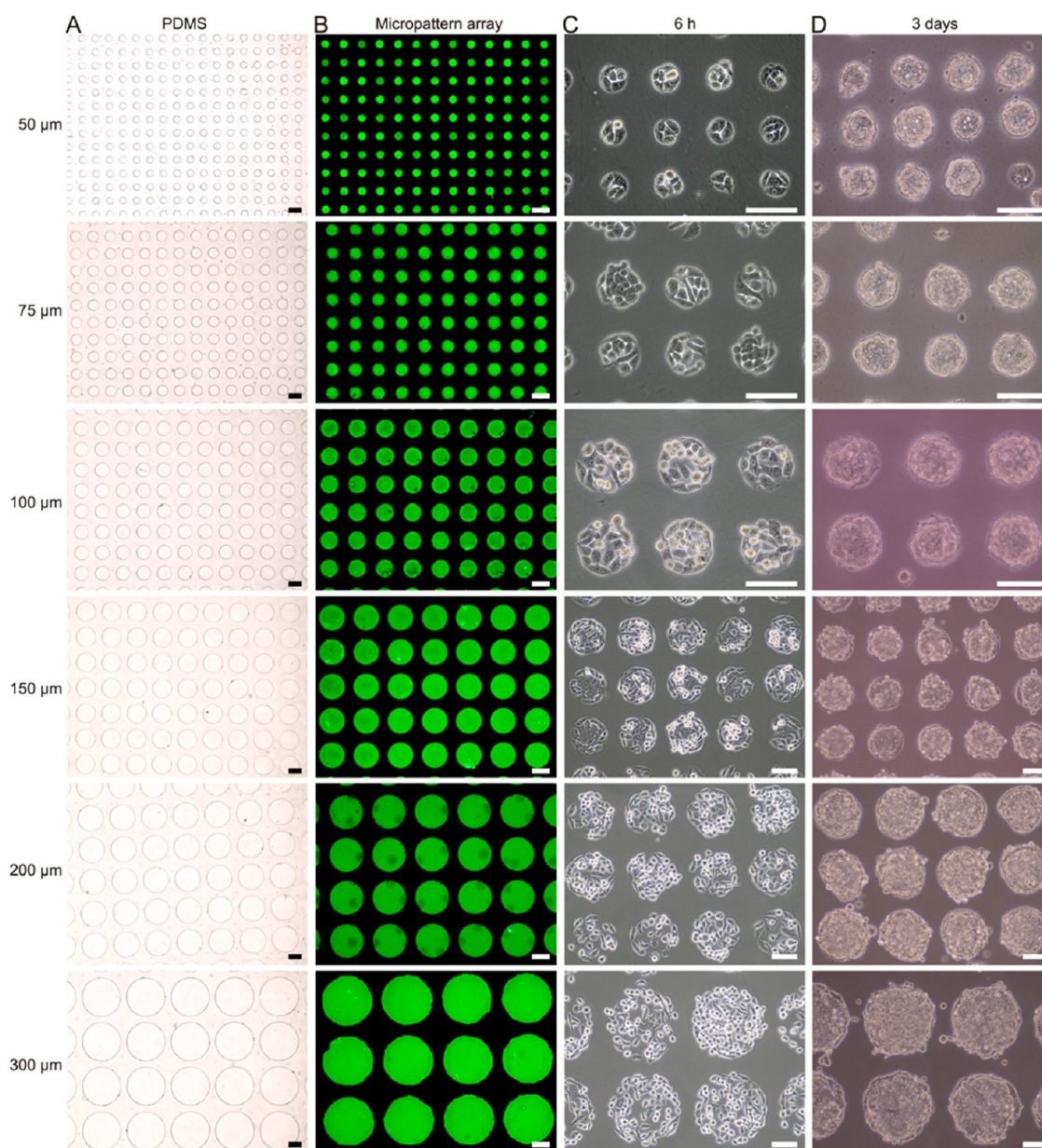
Figure 4. Fabrication of the round DLM micropattern array chips and the formation of 3D HepG2 cellular aggregates. (A) Round micropattern of PDMS seals with different diameters. (B) Proper homogeneous transfer of DLM fluorescently labeled to create round DLM micropattern array chips with different diameters. (C) Microscopic images of HepG2 cells cultured on round micropattern array chips with different diameters at 6 h. (D) Microscopic images of cellular aggregates cultured on round micropattern array chips with different diameters on day 3. Different diameters (50, 75, 100, 150, 200, and 300 μm). Scale bar = 100 μm.

platform for drug screening to evaluate the toxicity of paclitaxel, doxorubicin HCl, and disulfiram by fluorescence quantitative analysis. In general, the process of this study is shown in Figure 1.

2. RESULTS

2.1. Fabrication of DLM. The whole liver became white and translucent after decellularization (Figure 2A). The DNA content was 10671.2 ± 37.76 ng/mg in the normal tissue and 26.2 ± 1.83 ng/mg in the decellularized liver ($p < 0.05$) (Figure 2C). H&E (Figure 2B) and DAPI staining (Figure 2E) revealed no visible cell nuclei or cellular components in the decellularized livers. Scanning electron microscopy (SEM) images of the decellularized tissue revealed that the ECM ultrastructure was preserved (Figure 2D). Immunofluorescent

staining further revealed that major ECM proteins of the liver (Col I, Col IV, laminin, and fibronectin) were preserved in the matrix after decellularization (Figure 2G). Figure 3A,B shows that DLSs were powdered and digested to fabricate DLM. Mass spectrometry demonstrated that the DLM is composed of the $\alpha1$ and $\alpha2$ chains of collagen type I and $\alpha1$ chains of collagen type III (Figure 2F). The concentration of proteins presenting in the DLM solution (10 mg/mL) was 6.25 ± 0.34 mg/mL.

2.2. DLM as Coating Substrate for HepG2 Cell Culture. The DLM-coated substrate had a higher number of adhered cells after 4 h seeding than the other groups (Figure 3C). Similarly, the proliferation and viability of HepG2 cells cultured on DLM-coated substrates were significantly higher than other groups after culturing for 1 day (Figure 3D,E). The
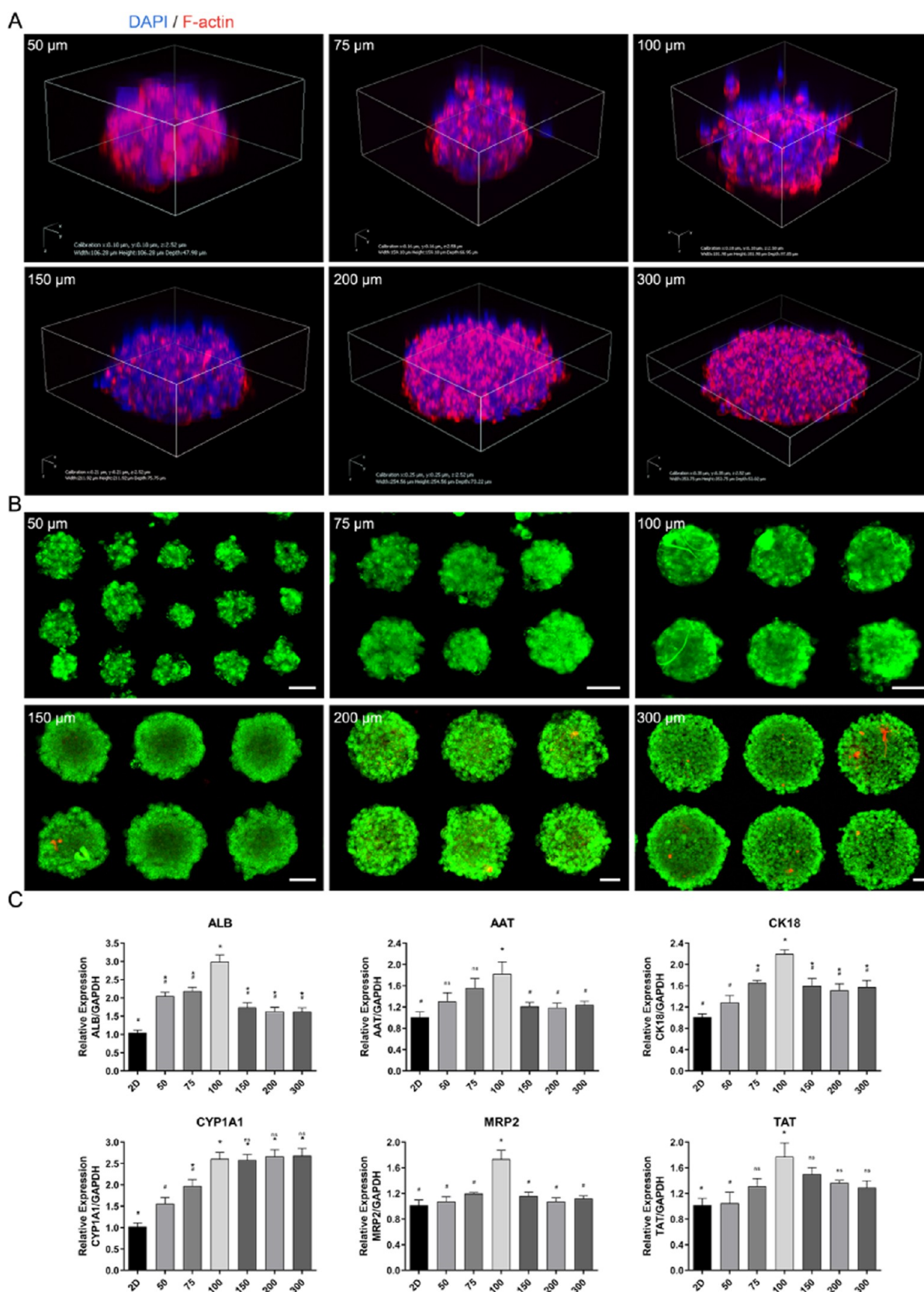
Figure 5. Evaluation of 3D HepG2 cellular aggregates of different sizes. (A) 3D view of cellular aggregates on the round DLM micropattern. (B) Live/Dead staining of cellular aggregates with different diameters cultured on round DLM micropattern array chips. Dead cells are stained red, while viable cells are stained green. Scale bar = 50 μm. (C) Gene expression levels of hepatic genes *alb*, *aat*, *ck*18, *cyp1a*1, *mrp*2, and *tat* were determined for different diameters compared to cells cultured on tissue culture plastic (TCP). *p <0.05, compared to the 2D, #p < 0.05, compared to the 100 μm, not significant (ns), compared to the 100 μm. Different diameters (50, 75, 100, 150, 200, and 300 μm).
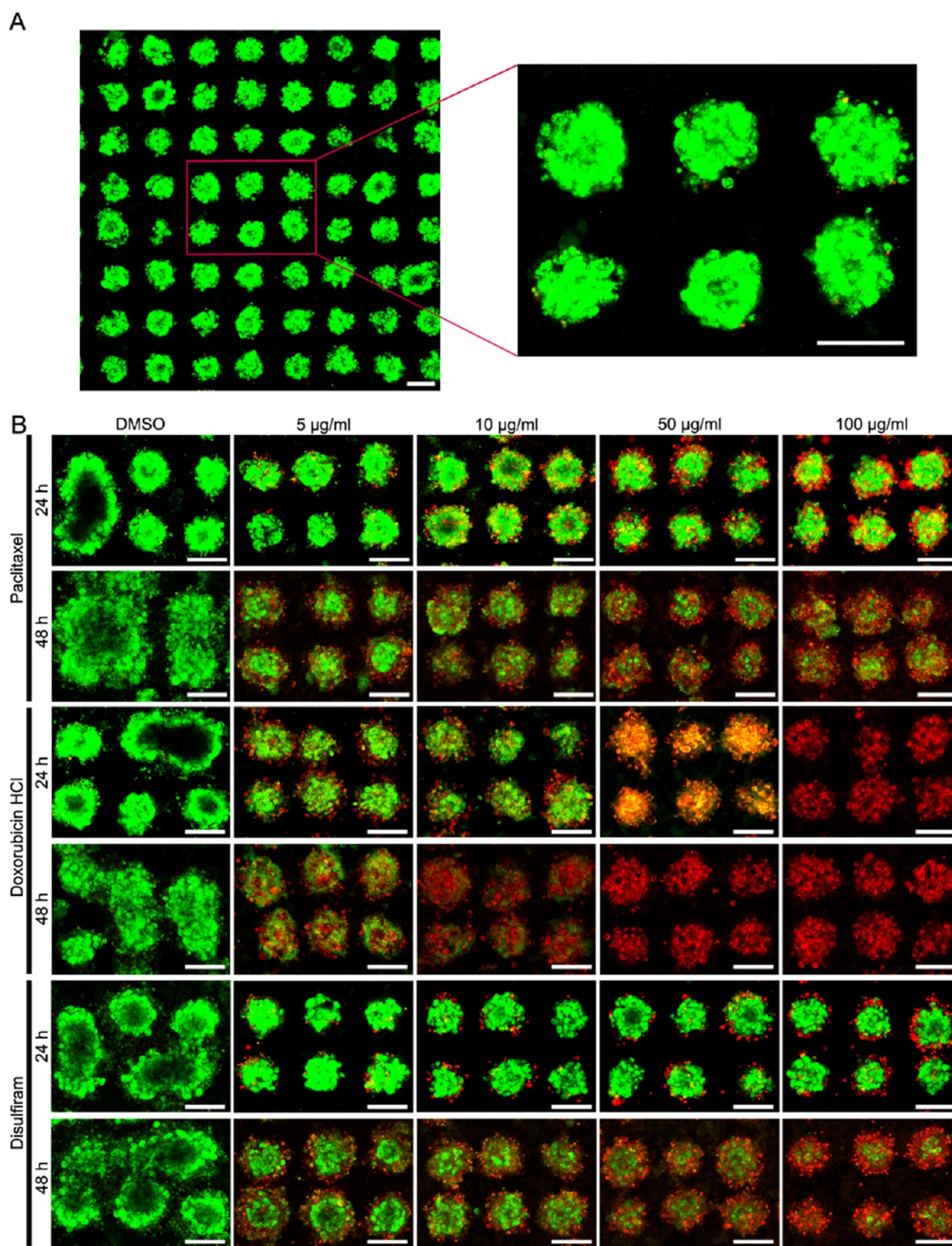
Figure 6. HepG2 spheroids cultured on DLM micropattern array chips (100 μm round micropattern) for anticancer drug screening. (A) Live/Dead staining of HepG2 spheroids before being treated with DMSO or drugs. (B) Live/Dead staining of HepG2 spheroids with various concentrations (5−100 μg/mL) of paclitaxel, doxorubicin HCl, and disulfiram. Scale bar = 100 μm.

HepG2 cells on the DLM-, Col I- and Matrigel-coated substrate showed a more flattened morphology due to strong adhesion, compared to the untreated substrate (Figure 3F). The albumin secretion and urea synthesis of HepG2 cells cultured on the DLM-coated substrate were significantly higher than those in other groups at all time points within 1 week (Figure 3G,H).

2.3. DLM Micropattern Array for Culturing 3D HepG2 Cellular Aggregates. Round and square PDMS micropatterns with different diameters absorbed the DLM solution to create specific uniform micropattern arrays on nontreated cell culture dishes (Figures 4A,B and S1A,B). Monolayer cells were restricted in micropattern array and further gradually formed 3D cellular aggregates through self-organization by the limitation of adhesive area and proliferation of cells. HepG2
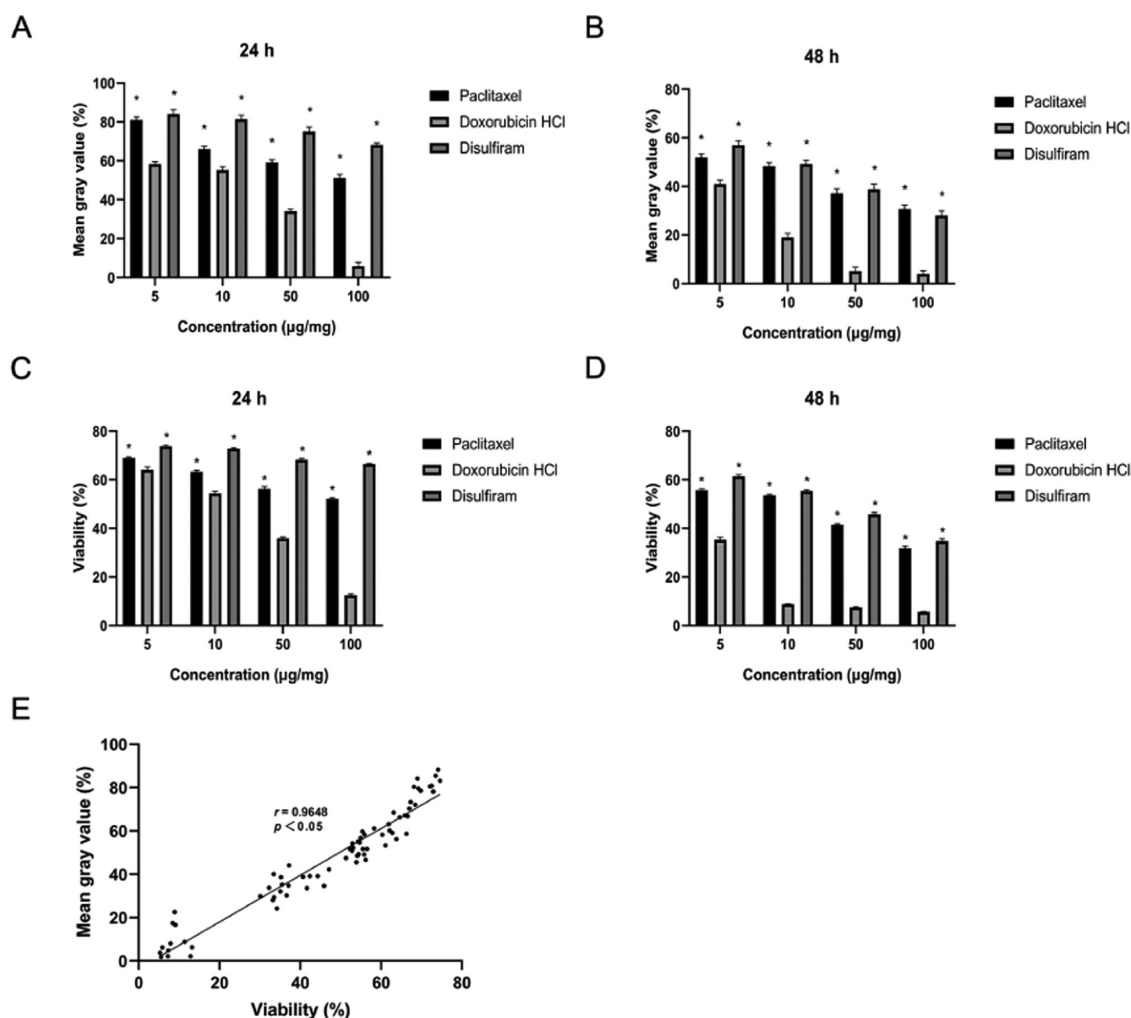
Figure 7. Quantitatively analyzing the efficacy of an anticancer drug. The viability of HepG2 spheroids (mean gray value) with various concentrations (5−100 μg/mL) of paclitaxel, doxorubicin HCl, and disulfiram at (A) 24 h and (B) 48 h and the viability of HepG2 spheroids (CCK-8) with various concentrations (5−100 μg/mL) of paclitaxel, doxorubicin HCl, and disulfiram at (C) 24 h and (D) 48 h (*$p < 0.05$, compared to doxorubicin HCl). (E) Correlation between mean gray value and viability detected by CCK-8 (r indicates correlation coefficient).

cells formed a monolayer at the microarray points after 6 h of seeding (Figures 4C and S1C). The average numbers of adherent cells on the round micropattern with diameters ranging from 50 to 300 μm were 3.89 ± 0.48, 11.56 ± 0.56, 19.33 ± 1.28, 30.56 ± 1.46, 39.11 ± 1.61, and 85.78 ± 1.61 cells (Figure S2A). The average numbers of adherent cells on the square micropattern with diameters ranging from 50 to 300 μm were 5.33 ± 0.47, 13.56 ± 0.53, 23.78 ± 0.72, 34.44 ± 0.96, 51.56 ± 1.83, and 101.11 ± 2.64 cells (Figure S2D). Size-controllable and arrangement-orderly cellular aggregates were subsequently observed on the DLM micropattern array chips at day 3. Interestingly, cellular aggregates derived from different geometric shapes of micropattern had quite different geometric topologies. For example, the round micropattern almost produced the round cellular aggregates (Figure 4D) and the square micropattern produced round or square cellular aggregates (Figure S1D). The cellular aggregates formed by square micropatterns (50 to 150 μm) had a round morphology accounting for 88.87 ± 1.44, 78.33 ± 2.53, 69.43 ± 2.94, and 42.77 ± 2.44%, while round cellular aggregates formed by 200 or 300 μm square micropatterns were not observed (Figure S2F). The average diameters of the cellular aggregates on the round micropattern with diameters ranging from 50 to 300 μm

were 61.46 ± 1.20, 74.06 ± 0.76, 97.02 ± 1.12, 148.15 ± 1.09, 195.40 ± 1.85, and 291.71 ± 1.17 μm (Figure S2B). The average diameters of the cellular aggregates on the square micropattern with diameters ranging from 50 to 300 μm were 71.23 ± 5.07, 97.83 ± 2.94, 115.60 ± 2.81, 157.36 ± 2.57, 210.91 ± 2.55, and 296.00 ± 2.14 μm (Figure S2E). These results indicated that the HepG2 cellular aggregates formed by round micropatterns had better geometric shape and size uniformity than those from square micropatterns. Cognizant of these, the round micropatterns were suitable for the formation of size-controllable and arrangement-orderly cellular aggregates.

2.4. Characteristics of 3D HepG2 Cellular Aggregates on the Round DLM Micropattern Array. HepG2 cells cultured on the round micropattern showed a multicellular geometry, cellular aggregates derived from different diameters of micropattern had quite different geometric topologies. Cellular aggregates cultured on the round micropattern with diameters ranging from 50 to 100 μm presented 3D spheroid's shape; cultured on the round micropattern with diameters ranging from 150 to 300 μm showed a flat plate with a hemispherical cap, which gradually became increasingly flat (Figure 5A). The average height of the cellular aggregates (Z-

axis) on the round micropattern with diameters ranging from 50 to 300 μm were 50.80 ± 1.77, 69.53 ± 1.53, 99.40 ± 1.45, 79.95 ± 2.22, 72.33 ± 3.66, and 55.67 ± 1.47 μm (Figure S2C). Consequently, 50−100 μm cellular aggregates were called spheroids. Almost no cell death was observed within HepG2 spheroids on the round micropattern with diameters ranging from 50 to 100 μm on day 3. However, the number of dead cells on the edge and inside of cellular aggregates gradually increased with increased cellular aggregates' diameter. Notably, significant cell death was on the edge and inside of 150, 200, and 300 μm cellular aggregates (Figure 5A). 2D cells and 50−300 μm cellular aggregates were collected for key gene expression analyses. The hepatic genes *alb*, *aat*, *ck*18, *cyp*1a1, *mrp*2, and *tat* were highly expressed in the 100 μm spheroids, which was significantly different from the 2D culture ($p < 0.05$); the genes *alb*, *ck*18, and *mrp*2 expressed in the 100 μm spheroids were significantly different from 50, 75, 150, 200, and 300 μm cellular aggregates ($p < 0.05$) (Figure 5B). These findings strongly suggested that the 100 μm spheroids with better viability and functions were the most suitable size. The 100 μm spheroids were formed on the round micropattern on the third day, but as the culturing time increased, the gap distance between spheroids gradually became smaller and adjacent spheroids were completely fused on the fifth day (Figure S3).

2.5. Drug Screening of HepG2 Spheroids on DLM Micropattern Arrays. HepG2 spheroids generated by the round DLM micropattern array chips with a diameter of 100 μm on day 3 were subjected to various concentrations of paclitaxel, doxorubicin HCl, and disulfiram (5−100 μg/mL) (Figures 6A,B and S4). In the negative control treated with 0.25% dimethyl sulfoxide (DMSO), the diameter of spheroids continued to increase and adjacent spheroids were further connected after 48 h, which did not occur in all chemotherapeutic groups. Compared to pretreatment, spheroids treated with an increase in the dose of doxorubicin HCl and incubated time had a looser structure with more dropped cells, while the morphology of spheroids treated with various concentrations of paclitaxel and disulfiram did not change significantly after 48 h (Figure S4).

For efficient and accurate drug screening, through the FluoroQuench fluorescent staining, the fluorescent images converted into gray images were automatically measured. The mean gray value representing the viability of the spheroids was further revealed to detect the drug efficiency. It can be observed that the cell death relied on the dose of drugs and incubated time. In all chemotherapeutic groups, for higher concentrations of drugs (50 and 100 μg/mL), the dead cells started to increase as soon as 24 h after incubated with drugs compared to lower drug concentrations (5 and 10 μg/mL); with an increase in incubated time, more and more cells on the spheroid surface died, followed by those inside the spheroids after 48 h in all chemotherapeutic groups (Figures 6B and 7A,B). The doxorubicin HCl treatment showed that the spheroids almost completely died at 24 h after being treated with 100 μg/mL doxorubicin HCl and at 48 h after being treated with 50 and 100 μg/mL doxorubicin HCl, and the viabilities were 5.83 ± 1.95, 5.07 ± 1.71 and 4.00 ± 1.27%, respectively (Figures 6B and 7A,B). However, for the paclitaxel and disulfiram treatment, the cells inside the spheroids did not die at 48 h after being treated with the highest concentration of drugs (100 μg/mL), and the viabilities were 30.60 ± 1.68 and 28.00 ± 1.87%, respectively (Figures 6B and 7B). The results

implied that doxorubicin HCl had a higher efficiency compared to paclitaxel and disulfiram. We next validated the authenticity of the above drug test results through CCK-8 (Figure 7C,D). The viability detected by CCK-8 was notably positively correlated with the mean gray value ($r = 0.9648$ and $p < 0.05$) (Figure 7E). These results suggested that the CCK-8 results were consistent with the FluoroQuench fluorescent staining results.

3. DISCUSSION

Tumor spheroids, as a 3D *in vitro* model, possess potentially predictive capacity for preclinical drug screening.[26] We have described modular and liver-specific micropattern array chips that allow us to efficiently fabricate large-scale, size-controllable, and arrangement-orderly HepG2 spheroids within 3 days. Our novel spheroid culture platform is composed of DLM and micropattern arrays. The DLM was obtained by the removal of cellular components and then grinding into powder, followed by enzymolysis to prepare the liver-specific bioink. Microcontact printing technology creates the limiting space, which can restrict the growth of cells to control the size and arrangement of spheroids, thus bringing convenience, reducing error, and increasing reproducibility for drug testing and screening. We demonstrated that the possibility of drug testing can be preliminarily, quickly, and directly analyzed by confocal microscopy analyzing fluorescence intensity on our chips, which eliminates the need for extracting the formed tumor spheroids and then performing the analysis in a separate well plate.

Currently, several cell spheroid culture methods have been developed. The common hanging drop culture method takes advantage of the gravitational force to induce the cellular auto-assembly, and the microwell technique uses low-surface-energy materials as coating materials, which reduce the cell−substrate interaction to facilitate the formation of spheroids.[27−29] The size of spheroids from these spheroid culture methods can be roughly controlled by introducing a defined numbers of cells to each droplet or microwell, which is labor-intensive and difficult to achieve on a large scale with a wide diameter variation and irregular morphology of spheroids.[30] Rocker system, through rocking, prevents cell sedimentation, promotes mixing and oxygenation, and increases the frequency of collisions between cells, thereby generating large-scale spheroids of different sizes.[31] Herein, micropattern arrays offer unique advantages over these spheroid culture methods to overcome the above difficulties. The diameter coefficient of variation was less than 6% (round micropatterns) by micropattern arrays. The diameter coefficient of variation of manner mouse mesenchymal stem cell (MSC) spheroids is just less than 10% by the automatic hanging drop system.[27] Micropatterns of precise area can limit the growth of cells to spontaneously assemble into size-controllable and regularly morphologic spheroids in several simple operations (seeding cells and removing unattached cells). The validation and consistency of oxygen, nutrition, and drug transport are guaranteed by the precise control over the size of spheroids.[3] A 2 × 2 cm² micropattern (round 100 μm) array chip containing 1.44 × 10⁴ micropatterns could approximately fabricate 1.32 × 10⁴ spheroids at a generation rate of up to 91.80 ± 1.27% (Figure S5). Furthermore, different scale chips can be fabricated by combining the different specifications of PDMS seals with proper cell culture well plates and dishes. When printing micropattern arrays in the well plates, this high-throughput

culture platform can be combined with commercially available automated micro-/nanoinjection systems for testing hundreds of drugs in a plate.[26]

Micropattern arrays also have the advantage of achieving the orderly arrangement of spheroids, which brings convenience to observation and analysis with the development of light microscopy. For traditional 2D imaging, it is difficult to allow a full appreciation of the complexity of 3D structures.[32] Providentially, 3D imaging such as confocal imaging, high content imaging, and multiphoton microscopy brings the hope for automated high-throughput analysis.[32,33] For standard evaluation methods of drug efficacy, various typical chemical reagents, including MTT, MTS, Prussian blue, WST-8, and CCK-8, did not easily diffuse into 3D cellular aggregates.[2] DLM micropattern arrays system, used in combination with confocal microscopy analyzing based on fluorescence intensity converted to mean gray value, is highly advantageous for high-throughput system-based drug screening. This process could achieve automation and eliminate the need of chemical detection. Kim et al. developed a graphene oxide micropattern platform to uniformly generate HepG2 spheroids, whose drug efficacy could be assessed by simply monitoring decreases in spheroid size.[2] This platform was highly promising for rapid high-throughput drug screening. However, spheroid sizes did not accurately reflect the drug efficacy. Note that not all HepG2 spheroid sizes treated with drugs changed, such as paclitaxel and disulfiram. Compared to pretreatment, HepG2 spheroids treated with doxorubicin HCl had their sizes significantly decreased; however, when treated with paclitaxel and disulfiram, the morphology of spheroids did not change significantly (Figure S4). Through Live/Dead staining of HepG2 spheroids, there were significantly increased dead cells in HepG2 spheroids (Figure 6). Consequently, changes in spheroid sizes had limitations in drug efficacy testing. Fluorescence quantitative analysis could be promising to overcome the above problems.

Microcontact printing appears to be the most critical determinant of how well the micropattern arrays perform. For guaranteeing the quality control of the micropattern arrays and compliance with the Good Manufacturing Practices (GMP), some studies demonstrated that with the use of specific microcontact printing devices, printing micropattern arrays could be almost entirely automated.[34,35] The working principle of microcontact printing principally relies on cell adhesion to the ECM proteins, which is indispensable for many physiological activities.[13] Collagen and fibronectin have been described as the bioink of micropattern printing to study the interaction between cells and ECM proteins.[15,36] These single-component ECM proteins micropattern arrays were supposed to help restore the lost ECM of isolation of islets from their native microenvironment and mimic the pancreatic islet microenvironment.[18] Recent efforts have clarified that ECM proteins micropattern arrays have become an effective tool for the fabrication of transferable micropatterned cell sheets and obtainment of monoclonal cells.[16,37] In this report, we described the use of DLM as the bioink to create DLM micropattern array chips for the first time, which restored the liver microenvironment. Compared with single-component ECM molecules (collagen), which are created in the traditional micropattern arrays, DLM contains a variety of biomacromolecules such as Col I, Col IV, laminin, and fibronectin, which are predominant in the liver.[19,38] Meanwhile, compared with commercial Matrigel (a natural ECM), which is purified from

Engelbreth-Holm-Swarm mouse sarcoma, DLM maintains liver-specific proteins, growth factors, and cytokines.[22] A previous study also reported that 24 kinds of proteins exclusively identified in the DLM were absent in Col I and Matrigel.[39] Herein, we validated that the DLM coating matrix was more conducive to the survival, proliferation, adhesion, and functions of HepG2 cells than Col I and Matrigel.

Next, we demonstrated the effects of the shape and size of the micropattern on the morphology, viability, and functions of spheroids. Round and square microwells are widely used for the fabrication of spheroids, and the effect of the shape of micropattern on the formation of spheroids has hardly been explored thus far. Our data showed that both round and square micropatterns could form 3D cellular aggregates. However, the square micropattern was hard to accurately control the morphology and size of cellular aggregates; the cellular aggregate morphology was irregular and the diameter coefficient of variation was up to 21%. This finding may be associated with the spontaneous assembling of cellular aggregates. Previous studies revealed that in the culture system of microwell, with a diameter lower than 200 μm, the HepG2 spheroids were less prone to viability effects related to the size.[29] In contrast to these studies, we demonstrated that when the diameter of HepG2 spheroids was greater than 100 μm, there were more dead cells on the edge and inside of the HepG2 cellular aggregates in our platform. It is well known that cell necrosis usually occurs in the core of spheroids because of the poor supply of the oxygen and nutrients transported to spheroids through diffusion. In the culture system of the micropattern array, the gap distance between spheroids will modulate the spheroid properties.[19,40] Notably, when the diameter of spheroids is indeed determined, the decreased distance between spheroids induces hypoxic conditions.[19] Therefore, with a determined gap distance between spheroids, the oxygen availability may fail to meet the increased oxygen demand with increasing size of spheroids.

Herein, DLM micropattern array chips were successfully fabricated, followed by a quick fabrication of large-scale, size-controllable, and arrangement-orderly HepG2 spheroids for high-throughput drug screening. Nonetheless, this study was limited by several factors. It did not focus on multitype cell culturing despite reports that stromal cells and immune cells such as cancer-associated fibroblasts (CAF) and tumor-associated macrophages (TAM) play important roles in the tumor microenvironment.[41,42] Cognizant of this, multitype cell cultures could be considered in future studies to fully mimic the tumor microenvironment and enhance the drug screening accuracy. Moreover, patient-derived cancer cells might be cultured on this platform for personalized drug screening and therapeutic strategies in the future.

4. CONCLUSIONS

In this study, DLM-derived micropattern array chips were developed to fabricate large-scale, size-controllable, and arrangement-orderly HepG2 spheroids within 3 days for drug screening. A circular micropattern with a diameter of 100 μm was the optimal processing parameter to fabricate HepG2 spheroids with homogeneous morphology, high cell viability, and optimal hepatic functions. We demonstrated that this novel platform could be used for drug-susceptibility testing with great rapidity and convenience by fluorescence quantitative analysis. This methodology may be possible to apply in advancing personalized medicine and drug discovery.

5. MATERIALS AND METHODS

All experimental protocols were approved by the Institutional Animal Care and Use Committee (IACUC) and Animal Experiment Center of Sichuan University. All animals were cared for in accordance with the requirements of the Laboratory Animal Welfare Act and amendments thereof.

5.1. Decellularization of Porcine Liver. The hepatic portal vein of the porcine liver was cannulated, and blood was flushed out using heparin-phosphate buffer saline after harvesting the liver from the pig. The liver was then frozen and thawed. Triton X-100, sodium dodecyl sulfate (SDS), and PBS were perfused through the liver to remove the miscellaneous cells. The specific steps were as described previously.[43] The decellularized liver scaffolds (DLSs) were then cut into cubes $(1 \times 1 \times 1 \text{ cm}^3)$ for subsequent lyophilization.

5.2. Decellularization Assessment. *5.2.1. DNA Extraction and Quantification.* DNA was extracted from 10 mg of fresh and decellularized matrix samples (dry weight) using DNA extraction kit (Tiangen Biotech Corporation, Beijing, China). The samples were then quantified using a NanoDrop spectrophotometer (ND-2000c, Thermo).

5.2.2. Histological Analysis. Normal fresh and decellularized liver tissues were fixed in 4% paraformaldehyde at room temperature for 24 h. They were then dehydrated stepwise using ethanol, immersed in xylene, and embedded in paraffin. The tissues were then sectioned into 5 μm slides and stained with hematoxylin and eosin (H&E) and 4′,6-diamidino-2-phenylindole (DAPI).

5.2.3. Fluorescence Microscopy. Fluorescence microscopy was performed to determine whether collagen I, collagen IV, laminin, and fibronectin were retained in the decellularized matrices. The stained sections were permeabilized with 0.1% Triton X-100 for 15 min and then blocked with 2% bovine serum albumin PBS for 1 h. They were subsequently treated with collagen I (cat. no. ab6308, 1:200, Abcam), collagen IV (cat. no. ab6586, 1:500, Abcam), laminin (cat. no. ab11575, 1:100, Abcam), and fibronectin (cat. no. ab6328, 1:200, Abcam) overnight at 4 °C, followed by incubation with species-appropriate secondary antibodies (Invitrogen, 1:500) and DAPI counterstaining.

5.2.4. Scanning Electron Microscopy (SEM). Fresh and decellularized matrix samples were fixed in 2.5% glutaraldehyde at room temperature for 12 h, followed by rinsing in deionized water, dehydration via a graded ethanol series, and drying in a critical point dryer (HCP2; Hitachi, Tokyo, Japan). The samples were subsequently sputter-coated with gold before SEM imaging. Electron micrographs were obtained at 5.0 kV using a Hitachi S-4800 SEM (Hitachi).

5.3. Solubilization of DLSs. Lyophilized DLSs were powdered using the Wiley Mill (Retsch, MM400, Germany) and solubilized with 10% (w/w) pepsin (Sigma-Aldrich) in 0.01 M HCl through stirring at room temperature for 48 h. The DLM solution was then neutralized to a pH of 7.2−7.4 by adding 0.1 M NaOH.[44] Its final concentration was then adjusted to 10 mg/mL using 1× PBS.

5.4. Mass Spectrometry Analysis for the Biochemical Composition of DLM Solution. The proteins and peptides preserved in the DLM solution were identified using mass spectrometry. Liquid chromatography−tandem mass spectrometry (LC-MS/MS) analysis was performed using an integrated system composed of nano-LC (EASY-nLC 1200,

Thermo Fisher Scientific) and an MS/MS spectrometer (Orbitrap Fusion Lumos Tribrid, Thermo Fisher Scientific). Solutions containing pepsin-digested protein fragments were injected into the nano-LC-MS/MS system and subsequently separated on a C18-StageTip column. The mass spectra were acquired using the high collision dissociation (HCD) method. The sus scrofa subset of the UniProt database (http://www.uniprot.org) extended with the MaxQuant (Version1.6.2.6) common contaminants database was used for the database search.

5.5. Cell Culture. HepG2 cells were obtained from the National Infrastructure of Cell Line Resources (Beijing, China). They were maintained in MEM media (Gibco, China) and supplemented with 10% FBS (Gibco, Australia), 1% NEAA (Gibco), and 1% penicillin−streptomycin solution (HyClone, China) in a 5% CO_2 incubator (Thermo) at 37 °C.

5.6. DLM Coating and Assessment. Proteins present in the DLM solution (10 mg/mL) were quantified using a NanoDrop spectrophotometer. The solution was then diluted with PBS to a final protein concentration of 0.1 mg/mL. Col I (BD Biosciences, Bedford, MA) solution (0.1 mg/mL) and Matrigel (Corning) solution (0.1 mg/mL) were used as the control coating substances. Polystyrene plates were coated with the substances for 1 h at room temperature, followed by three washes with PBS. The uncoated PS substrate served as a negative control.[25] The cell adhesion percentage after 4 h of seeding was evaluated using Countess II FL (Invitrogen) counting of nonadhered cells. HepG2 cell proliferation was analyzed using the Cell Counting Kit-8 assay (CCK-8, MCE, China). Their viability on the coated substrates was examined using the FluoroQuench fluorescent stain (One Lambda; Thermo Fisher Scientific, Inc., Waltham, MA) following the manufacturer's protocol. Cell viability was determined by calculating the ratio of live cells to the total cell populations. The functions of the different coating matrices were analyzed by seeding HepG2 cells on coated 24-well culture plates at a rate of 2.5×10^4 cells per well. The culture media were changed daily, and the cells were retrieved on days 1, 3, 5, and 7 to determine their ureagenesis and albumin synthesis capacity. Albumin levels and urea concentration were determined using ELISA kits (ab179887; Abcom) and the QuantiChrom urea assay kit (DIUR-500; Bioassay), respectively.

5.7. Micropattern Array Printing. Poly-(dimethylsiloxane) (PDMS) seals were obtained through laser etching of the characteristic pattern on a silicon wafer. Round and square micropatterns with diameters of 50, 75, 100, 150, 200, 300 μm and 50 μm spacing between micropatterns were used as the templates. The seal surface was coated with 0.1 mg/mL DLM solution and 2 μg of fluorescein isothiocyanate isomer for 20 min at room temperature. Excess DLM solution was drained, and the seals were dried at 37 °C for 10 min. The coated seals were stacked with a 35 mm diameter nontreated cell culture dish at a 0.2 N force for 10 min.[16] The shapes of the microarray arrays were subsequently observed under a fluorescence microscope (OBSERVER D1/AX10 cam HRC, CARL ZEISS, Germany). The treated dishes were coated with 10 g/L pluronic F- 127 water solution (Sigma) for 1 h to prevent nonspecific cellular adherence and then sterilized through ultraviolet irradiation for 1 h.

5.8. 3D Cellular Aggregates Culture. HepG2 cells (2×10^5) were seeded on DLM-patterned dishes containing 3 mL of MEM media to have an equal cell density on the

micropatterned dishes. The culture media was sucked out after 6 h, and the dishes were washed thrice with PBS to remove the unattached cells. The cellular aggregates' morphology at 6 h and on days 1, 2, 3, 4, 5, and 6 after seeding was observed and imaged using EVOS XL Core (Invitrogen), and their diameters were analyzed using the ImageJ software (National Institutes of Health, Bethesda, MD). Their viability was assessed through FluoroQuench fluorescent staining followed by imaging using a confocal microscope (N-STORM & A1, Nikon, Japan). Cellular aggregates grown on micropatterned dishes were fixed with 4% formaldehyde for 20 min at room temperature, stained with rhodamine phalloidin solution (100 nM) (Cytoskeleton) for 45 min at room temperature, and counterstained with DAPI. Fluorescent images were acquired with a two-photon confocal microscope (A1RMP+, Nikon, Japan).

5.9. Quantitative Real-Time PCR (RT-PCR). Total RNA was extracted from the cellular aggregates using the TRIzol reagent (category number 15596-026, Invitrogen) following the manufacturer's instructions. Complementary DNA (cDNA) was then synthesized from 1 μg of total RNA using the iScript cDNA Synthesis Kit (Bio-Rad). Quantitative PCR reactions for hepatocyte genes *alb*, *aat*, *ck*18, *cyp1a1*, *mrp2*, and *tat* were performed using the SsoFast EvaGreen Supermix Kit (Bio-Rad) following the manufacturer's instructions. The glyceraldehyde-3-phosphate dehydrogenase (GAPDH) housekeeping gene was used as an endogenous internal control. The PCR reactions were performed in triplicate followed by gene expression analysis and quantification using the Stratagene analysis software and the $2^{-\Delta\Delta Ct}$ method, respectively.

5.10. Chemotherapeutic Drug Cytotoxicity Screening. The HepG2 spheroids were incubated with paclitaxel, doxorubicin HCl, and disulfiram at different concentrations (5, 10, 50, and 100 μg/mL) for 24 and 48 h. Spheroids were incubated with 0.25% DMSO as the negative control. The morphology of spheroids at 24 and 48 h was observed and imaged using EVOS XL Core. The viability of spheroids was assessed using the FluoroQuench fluorescent staining followed by imaging using a confocal microscope, and the fluorescence intensity was measured as a mean gray value and analyzed by ImageJ software for the quantification of the viability of spheroids. Cell viability was also assessed after 24 and 48 h of treatment using a CCK-8 to determine their survival rate.

5.11. Data Analysis. All data were analyzed using the SPSS statistical software (version 17.0) and presented as mean ± SEM. The datasets were subjected to one-way analysis of variance (ANOVA) for multiple comparisons. The Dunnett *t*-test was used to compare datasets between two groups. Correlations were determined by Pearson correlation; *p* < 0.05 indicated significant differences between groups.

ASSOCIATED CONTENT

Ⓢ Supporting Information

The Supporting Information is available free of charge at https://pubs.acs.org/doi/10.1021/acsomega.1c06302.

> Fabrication of the square DLM micropattern array chips and the formation of 3D HepG2 cellular aggregates (Figure S1); parameters of HepG2 cellular aggregates' morphological character on round and square micropatterns (Figure S2); HepG2 spheroid formation process and culturing on 100 μm round micropattern

array chips for 6 days (Figure S3); HepG2 spheroids cultured on DLM micropattern array chips (100 μm round micropattern) for anticancer drug screening (Figure S4); generation rate of HepG2 spheroids on DLM micropattern array chips (Figure S5) (PDF)

AUTHOR INFORMATION

Corresponding Author

Ji Bao − *Institute of Clinical Pathology, Key Laboratory of Transplant Engineering and Immunology, NHC, West China Hospital, Sichuan University, Chengdu 610041 Sichuan Province, China;* ⓞ orcid.org/0000-0001-8413-3270; Email: baoji@scu.edu.cn

Authors

Xinglong Zhu − *Institute of Clinical Pathology, Key Laboratory of Transplant Engineering and Immunology, NHC, West China Hospital, Sichuan University, Chengdu 610041 Sichuan Province, China*

Qiong Wu − *Institute of Clinical Pathology, Key Laboratory of Transplant Engineering and Immunology, NHC, West China Hospital, Sichuan University, Chengdu 610041 Sichuan Province, China; Laboratory of Liver Transplantation, Frontiers Science Center for Disease-related Molecular Network, West China Hospital, Sichuan University, Chengdu 610041 Sichuan Province, China*

Yuting He − *Institute of Clinical Pathology, Key Laboratory of Transplant Engineering and Immunology, NHC, West China Hospital, Sichuan University, Chengdu 610041 Sichuan Province, China*

Mengyu Gao − *Institute of Clinical Pathology, Key Laboratory of Transplant Engineering and Immunology, NHC, West China Hospital, Sichuan University, Chengdu 610041 Sichuan Province, China; Department of Pathology, West China Hospital, Sichuan University, Chengdu 610041 Sichuan Province, China*

Yi Li − *Institute of Clinical Pathology, Key Laboratory of Transplant Engineering and Immunology, NHC, West China Hospital, Sichuan University, Chengdu 610041 Sichuan Province, China; Precision Medicine Key Laboratory, West China Hospital, Sichuan University, Chengdu 610041, China*

Wanliu Peng − *Institute of Clinical Pathology, Key Laboratory of Transplant Engineering and Immunology, NHC, West China Hospital, Sichuan University, Chengdu 610041 Sichuan Province, China*

Shengfu Li − *Key Laboratory of Transplant Engineering and Immunology, NHC, West China Hospital, Sichuan University, Chengdu 610041 Sichuan Province, China*

Yong Liu − *Department of Burn and Plastic Surgery, West China Hospital, Sichuan University, Chengdu 610041 Sichuan Province, China*

Rundong Zhang − *West China School of Medicine, Sichuan University, Chengdu 610041 Sichuan Province, China*

Complete contact information is available at:
https://pubs.acs.org/10.1021/acsomega.1c06302

Author Contributions

○X.Z. and Q.W. contributed equally to this work.

Notes

The authors declare no competing financial interest.

REFERENCES

(1) Islami, F.; Miller, K. D.; Siegel, R. L.; Fedewa, S. A.; Ward, E. M.; Jemal, A. Disparities in liver cancer occurrence in the United States by race/ethnicity and state. *Ca-Cancer J. Clin.* 2017, *67*, 273−289.

(2) Kim, C. H.; Suhito, I. R.; Angeline, N.; Han, Y.; Son, H.; Luo, Z.; Kim, T. H. Vertically Coated Graphene Oxide Micro-Well Arrays for Highly Efficient Cancer Spheroid Formation and Drug Screening. *Adv. Healthcare Mater.* 2020, *9*, No. e1901751.

(3) Jo, Y.; Choi, N.; Kim, K.; Koo, H.-J.; Choi, J.; Kim, H. N. Chemoresistance of Cancer Cells: Requirements of Tumor Micro-environment-mimicking In Vitro Models in Anti-Cancer Drug Development. *Theranostics* 2018, *8*, 5259−5275.

(4) Laschke, M. W.; Menger, M. D. Life is 3D: Boosting Spheroid Function for Tissue Engineering. *Trends Biotechnol.* 2017, *35*, 133−144.

(5) Nath, S.; Devi, G. R. Three-dimensional culture systems in cancer research: Focus on tumor spheroid model. *Pharmacol. Ther.* 2016, *163*, 94−108.

(6) Eilenberger, C.; Rothbauer, M.; Ehmoser, E.-K.; Ertl, P.; Küpcü, S. Effect of Spheroidal Age on Sorafenib Diffusivity and Toxicity in a 3D HepG2 Spheroid Model. *Sci. Rep.* 2019, *9*, No. 4863.

(7) de Wever, O.; Härmä, V.; Schukov, H.-P.; Happonen, A.; Ahonen, I.; Virtanen, J.; Siitari, H.; Åkerfelt, M.; Lötjönen, J.; Nees, M. Quantification of Dynamic Morphological Drug Responses in 3D Organotypic Cell Cultures by Automated Image Analysis. *PLoS One* 2014, *9*, No. e96426.

(8) Verjans, E.-T.; Doijen, J.; Luyten, W.; Landuyt, B.; Schoofs, L. Three-dimensional cell culture models for anticancer drug screening: Worth the effort? *J. Cell. Physiol.* 2018, *233*, 2993−3003.

(9) Huang, B. W.; Gao, J. Q. Application of 3D cultured multicellular spheroid tumor models in tumor-targeted drug delivery system research. *J. Controlled Release* 2018, *270*, 246−259.

(10) Li, Y.; Wu, Q.; Yang, Z.; He, Y.; Weng, C.; Gao, M.; Zhang, B.; Wang, Y.; Li, L.; Chen, F.; et al. Heterotopic vascularization and functionalization of implantable bio engineered hepatic tissue alleviates liver injury in rats. *Liver Int.* 2020, *40*, 712−726.

(11) Perez, J. E.; Nagle, I.; Wilhelm, C. Magnetic molding of tumor spheroids: emerging model for cancer screening. *Biofabrication* 2020, *13*, No. 015018.

(12) Wei, L. N.; Chua, C. K.; Shen, Y. F. Print Me An Organ! Why We Are Not There Yet. *Prog. Polym. Sci.* 2019, *97*, No. 101145.

(13) Hu, S.; Chen, T. H.; Zhao, Y.; Wang, Z.; Lam, R. H. W. Protein-Substrate Adhesion in Microcontact Printing Regulates Cell Behavior. *Langmuir* 2018, *34*, 1750−1759.

(14) Li, S.; Yang, K.; Chen, X.; Zhu, X.; Zhou, H.; Li, P.; Chen, Y.; Jiang, Y.; Li, T.; Qin, X.; et al. Simultaneous 2D and 3D cell culture array for multicellular geometry, drug discovery and tumor micro-environment reconstruction. *Biofabrication* 2021, *13*, No. 045013.

(15) Wang, Z.; Lang, B.; Qu, Y.; Li, L.; Song, Z.; Wang, Z. Single-cell patterning technology for biological applications. *Biomicrofluidics* 2019, *13*, No. 061502.

(16) Zhang, Y.; Gao, M.; Hu, M.; Zhang, B.; He, Y.; Li, S.; Bao, J.; Bu, H. Using the Patterned Microarray Culture to Obtain Gene-Editing Monoclonal Cells. *Transplant. Proc.* 2020, *52*, 1906−1909.

(17) Tanaka, N.; Ota, H.; Fukumori, K.; Miyake, J.; Yamato, M.; Okano, T. Micro-patterned cell-sheets fabricated with stamping-force-controlled micro-contact printing. *Biomaterials* 2014, *35*, 9802−9810.

(18) Hadavi, E.; Leijten, J.; Brinkmann, J.; Jonkheijm, P.; Karperien, M.; van Apeldoorn, A. Fibronectin and Collagen IV Microcontact Printing Improves Insulin Secretion by INS1E Cells. *Tissue Eng., Part C* 2018, *24*, 628−636.

(19) Miyamoto, D.; Hara, T.; Hyakutake, A.; Nakazawa, K. Changes in HepG2 spheroid behavior induced by differences in the gap distance between spheroids in a micropatterned culture system. *J. Biosci. Bioeng.* 2018, *125*, 729−735.

(20) Choudhury, D.; Tun, H. W.; Wang, T.; Naing, M. W. Organ-Derived Decellularized Extracellular Matrix: A Game Changer for Bioink Manufacturing? *Trends Biotechnol.* 2018, *36*, 787−805.

(21) Kabirian, F.; Mozafari, M. Decellularized ECM-derived bioinks: Prospects for the future. *Methods* 2020, *171*, 108−118.

(22) Saldin, L. T.; Cramer, M. C.; Velankar, S. S.; White, L. J.; Badylak, S. F. Extracellular matrix hydrogels from decellularized tissues: Structure and function. *Acta Biomater.* 2017, *49*, 1−15.

(23) Badileanu, A.; Mora-Navarro, C.; Martins, A.; Garcia, M. E.; Freytes, D. O.; et al. Fast Automated Approach for the Derivation of Acellular Extracellular Matrix Scaffolds from Porcine Soft Tissues. *ACS Biomater. Sci. Eng.* 2020, *6*, 4200−4213.

(24) Multhaupt, H. A. B.; Leitinger, B.; Gullberg, D.; Couchman, J. R. Extracellular matrix component signaling in cancer. *Adv. Drug Delivery Rev.* 2016, *97*, 28−40.

(25) Lee, J. S.; Shin, J.; Park, H. M.; Kim, Y. G.; Kim, B. G.; Oh, J. W.; Cho, S. W. Liver extracellular matrix providing dual functions of two-dimensional substrate coating and three-dimensional injectable hydrogel platform for liver tissue engineering. *Biomacromolecules* 2014, *15*, 206−218.

(26) Ganguli, A.; Mostafa, A.; et al. Three-dimensional microscale hanging drop arrays with geometric control for drug screening and live tissue imaging. *Sci. Adv.* 2021, *7*, No. eabc1323.

(27) Kim, S. J.; Kim, E. M.; Yamamoto, M.; Park, H.; Shin, H. Engineering Multi-Cellular Spheroids for Tissue Engineering and Regenerative Medicine. *Adv. Healthcare Mater.* 2020, *9*, No. 2000608.

(28) Chao, C.; Le, P. N.; Engelward, B. P. SpheroidChip: Patterned Agarose Microwell Compartments Harboring HepG2 Spheroids are Compatible with Genotoxicity Testing. *ACS Biomater. Sci. Eng.* 2020, *6*, 2427−2439.

(29) Elien, G.; Laurent, D.; Thomas, B.; Peter, D.; Leo, V. G.; Aart, V. A.; Ria, C.; Michiya, M. High Throughput Micro-Well Generation of Hepatocyte Micro-Aggregates for Tissue Engineering. *PLoS One* 2014, *9*, No. e105171.

(30) Shen, H.; Cai, S.; Wu, C.; Yang, W.; Yu, H.; Liu, L. Recent Advances in Three-Dimensional Multicellular Spheroid Culture and Future Development. *Micromachines* 2021, *12*, 96.

(31) Brophy, C. M.; Luebke-Wheeler, J. L.; Amiot, B. P.; Khan, H.; Remmel, R. P.; Rinaldo, P.; Nyberg, S. L. Rat hepatocyte spheroids formed by rocked technique maintain differentiated hepatocyte gene expression and function. *Hepatology* 2009, *49*, 578−586.

(32) Rios, A. C.; Clevers, H. Imaging organoids: a bright future ahead. *Nat. Methods* 2018, *15*, 24−26.

(33) Renner, H.; Grabos, M.; Becker, K. J.; Kagermeier, T. E.; Wu, J.; Otto, M.; Peischard, S.; Zeuschner, D.; TsyTsyura, Y.; Disse, P.; et al. A fully automated high-throughput workflow for 3D-based chemical screening in human midbrain organoids. *eLife* 2020, *9*, No. e52904.

(34) Bou Chakra, E.; Hannes, B.; Vieillard, J.; Mansfield, C. D.; Mazurczyk, R.; Bouchard, A.; Potempa, J.; Krawczyk, S.; Cabrera, M. Grafting of antibodies inside integrated microfluidic-microoptic devices by means of automated microcontact printing. *Sens. Actuators, B* 2009, *140*, 278−286.

(35) Elloumi-Hannachi, I.; Maeda, M.; Yamato, M.; Okano, T. Portable microcontact printing device for cell culture. *Biomaterials* 2010, *31*, 8974−8979.

(36) Huebsch, N.; Arany, P. R.; Mao, A. S.; Shvartsman, D.; Ali, O. A.; Bencherif, S. A.; Rivera-Feliciano, J.; Mooney, D. J. Harnessing traction-mediated manipulation of the cell/matrix interface to control stem-cell fate. *Nat. Mater.* 2010, *9*, 518−526.

(37) Elloumi Hannachi, I.; Itoga, K.; Kumashiro, Y.; Kobayashi, J.; Yamato, M.; Okano, T. Fabrication of transferable micropatterned-co-cultured cell sheets with microcontact printing. *Biomaterials* **2009**, *30*, 5427−5432.

(38) Mattei, G.; Di Patria, V.; Tirella, A.; Alaimo, A.; Elia, G.; Corti, A.; Paolicchi, A.; Ahluwalia, A. Mechanostructure and composition of highly reproducible decellularized liver matrices. *Acta Biomater.* **2014**, *10*, 875−882.

(39) Li, Q.; Uygun, B. E.; Geerts, S.; Ozer, S.; Scalf, M.; Gilpin, S. E.; Ott, H. C.; Yarmush, M. L.; Smith, L. M.; Welham, N. V.; et al. Proteomic analysis of naturally-sourced biological scaffolds. *Biomaterials* **2016**, *75*, 37−46.

(40) Byun, H.; Bin Lee, Y.; Kim, E. M.; Shin, H. Fabrication of size-controllable human mesenchymal stromal cell spheroids from micro-scaled cell sheets. *Biofabrication* **2019**, *11*, No. 035025.

(41) Meurette, O.; Mehlen, P. Notch Signaling in the Tumor Microenvironment. *Cancer Cell* **2018**, *34*, 536−548.

(42) Gencoglu, M. F.; Barney, L. E.; Hall, C. L.; Brooks, E. A.; Schwartz, A. D.; Corbett, D. C.; Stevens, K. R.; Peyton, S. R. Comparative Study of Multicellular Tumor Spheroid Formation Methods and Implications for Drug Screening. *ACS Biomater. Sci. Eng.* **2018**, *4*, 410−420.

(43) Wu, Q.; Bao, J.; Zhou, Y. J.; Wang, Y. J.; Du, Z. G.; Shi, Y. J.; Li, L.; Bu, H. Optimizing perfusion-decellularization methods of porcine livers for clinical-scale whole-organ bioengineering. *BioMed. Res. Int.* **2015**, *2015*, No. 785474.

(44) Wang, W.; Zhang, X.; Chao, N. N.; Qin, T. W.; Ding, W.; Zhang, Y.; Sang, J. W.; Luo, J. C. Preparation and characterization of pro-angiogenic gel derived from small intestinal submucosa. *Acta Biomater.* **2016**, *29*, 135−148.